IBS Center
for Climate Physics

EGU General Assembly 2020

Ultra-high-resolution future coupled model projections of atmospheric rivers

Arjun Babu Nellikkattil[1,2], Bin Guan[3,4], June-Yi Lee[1,2,5], Axel Timmermann[1,2], Sun-Seon Lee[1], Duane Waliser[3], Jung-Eun Chu[1]

Center for Climate Physics, Institute for Basic Science, Busan, South Korea[1]
Department of Climate System, Pusan National University, Busan, South Korea[2]
Jet Propulsion Laboratory, California Institute of Technology[3]
Joint Institute for Regional Earth System Science and Engineering, University of California, Los Angeles [4]
Research Center for Climate Sciences, Pusan National University, Busan, South Korea[5]

Introduction & Motivation

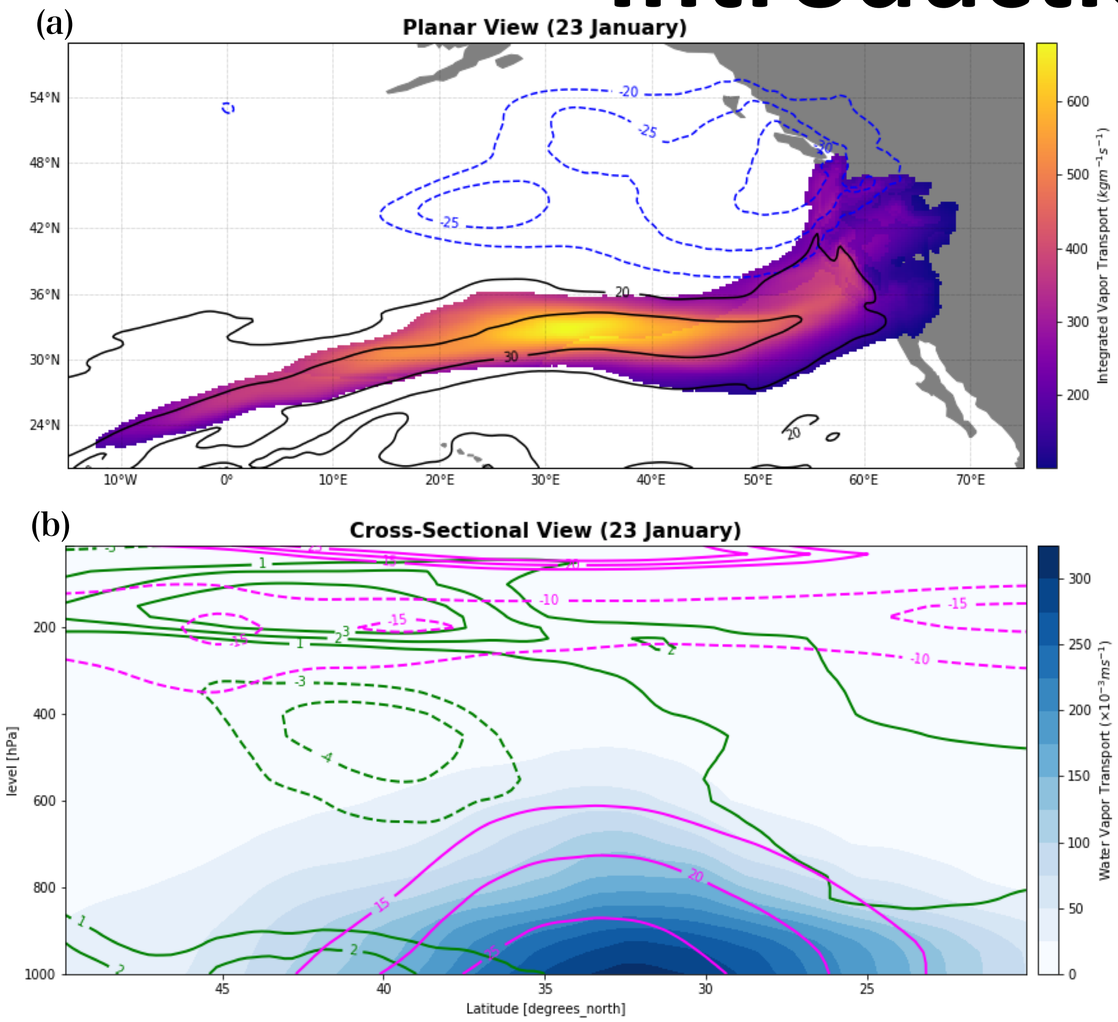

Figure 1: An example of a detected AR in CESM1.2.2 high-resolution simulation for present day conditions. (a) shows the detected shape with filled contours indicating the integrated water vapor transport. The black contours represents the total precipitable water in kg/m^2 while the blue contours shows the surface pressure anomaly. (b) is the latitudinal cross section of AR in (a). The filled contours represent the water vapor transport. The magenta and green contours are the anomalous horizontal wind(ms^{-1}) and air temperature(K) respectively.

1. Atmospheric Rivers (ARs) are defined as a long narrow region of strong horizontal water vapor transport[1].
2. At any instant of time ARs transport significant quantity of total water vapor transport across subtropics[2].
3. ARs play a significant role in the mean and well as extreme precipitation along the coastal regions where they make landfalls[3].
4. Although AR are manifested as a large-scale synoptic weather phenomenon, they interact significantly with the topography which is better resolved in a ultra-high resolution simulation.
5. A high-resolution modeling framework is also expected to provide a more realistic precipitation patterns[4].
6. In this analysis, we show response of AR to enhanced GHG forcing using two different value of thresholds.

Data and Methods

To detect ARs, we followed [5]. As evident from the definition an AR should have high (Integrated Vapor Transport) IVT and should satisfy a certain geometric criterion with considerable amount of coherent poleward transport. Where IVT is defined as,

$$IVT = \sqrt{(IVT_x + IVT_y)^2} \quad \text{and,} \quad IVT_x = \frac{-1}{g}\int_{1000hpa}^{300hpa} Uq, \quad IVT_x = \frac{-1}{g}\int_{1000hpa}^{300hpa} Vq$$

a. The threshold: A point is identified as part of an atmospheric river if the IVT is greater than the 85th percentile of daily IVT values taken over a period of 5 months centered on the current month at the grid point or 100 $kgm^{-1}s^{-1}$, whichever is larger.

b. The Geometry: Once the points of higher than threshold IVT is identified, only those structures which have a length to width ratio higher than 2 is identified as atmospheric river. Structures with length less than 2000 km and width less than 1000 km are not considered

c. The Direction: Structures that deviate by more than 45^0 from the mean direction is also removed from the analysis. Those structures without a significant poleward transport (50 $kgm^{-1}s^{-1}$) is also removed.

d. Landfall: Rivers identified in the previous three steps are examined to see if they cross a grid point with land fraction > 0.5. These will be identified as landfalling atmospheric rivers.

Datasets Used:

To detect ARs we used daily mean Horizontal Velocity (U,V) and Specific humidity (q) and land-sea mask from the following datasets

1. Fully coupled CESM1.2.2 High Resolution Simulation: The atmospheric component was simulated with a horizontal resolution of around 0.25° and 30 vertical layers. We conducted three experiments with different level of fixed greenhouse gas condition: (1) present-day (PD) (CO2 concentration of 367 ppm), (2) doubling CO_2 (2CO2)(734 ppm), and (3) quadrupling CO_2(4CO2) (1468 ppm). AR detection algorithm is run on the 20 year period after letting the model run for 70, 80 and 80 years respectively.

Validation

Source: Guan and Waliser (2015)

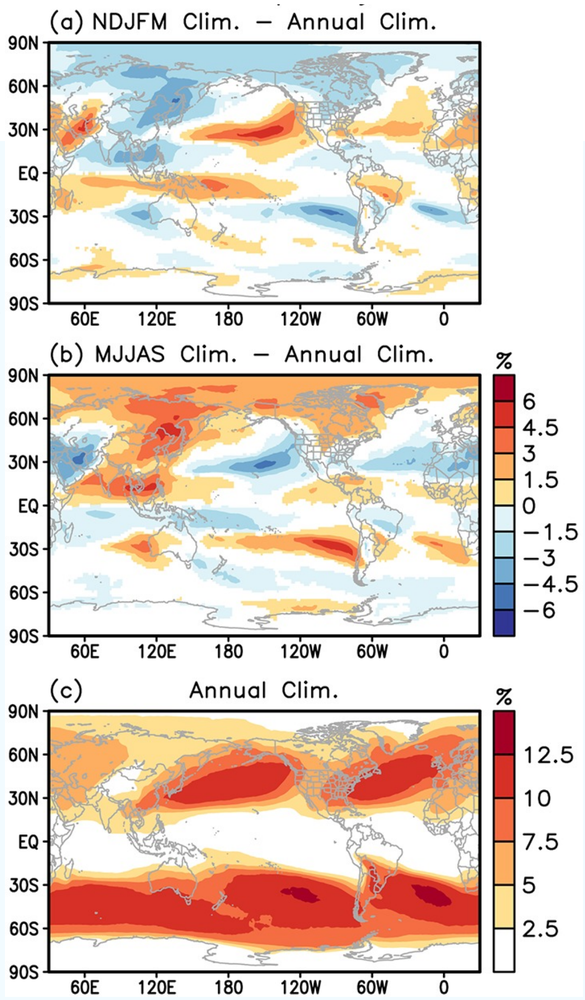

ERA-Interim (1979-2014)

Figure 3: (a–c) AR frequency (percent of time steps) in (Figure 3a) NDJFM (November-March) and (Figure 3b) MJJAS (May to September with (Figure 3c) the annual AR frequency subtracted. In Figures 3a, 3b values are shown only if they are statistically significant at the 95% level. The calculation were made using ERA-Interim data 6 hourly data for the period of 1997–2014

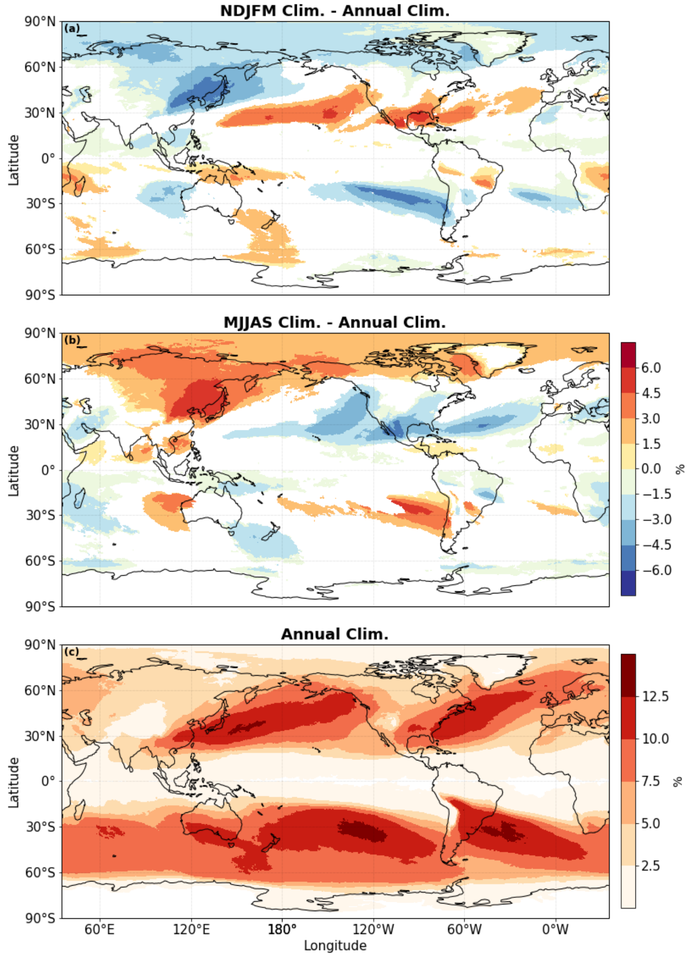

CESM1.2.2 Hi-Res (20 Years)

Figure 4: Same as shown in figure 3 but for daily mean CESM ultra high resolution

- CESM1.2.2 high resolution run can simulate realistic AR frequency with reasonably well.
- The southern Indian ocean has less AR days compared to the observations

Choosing IVT Thresholds

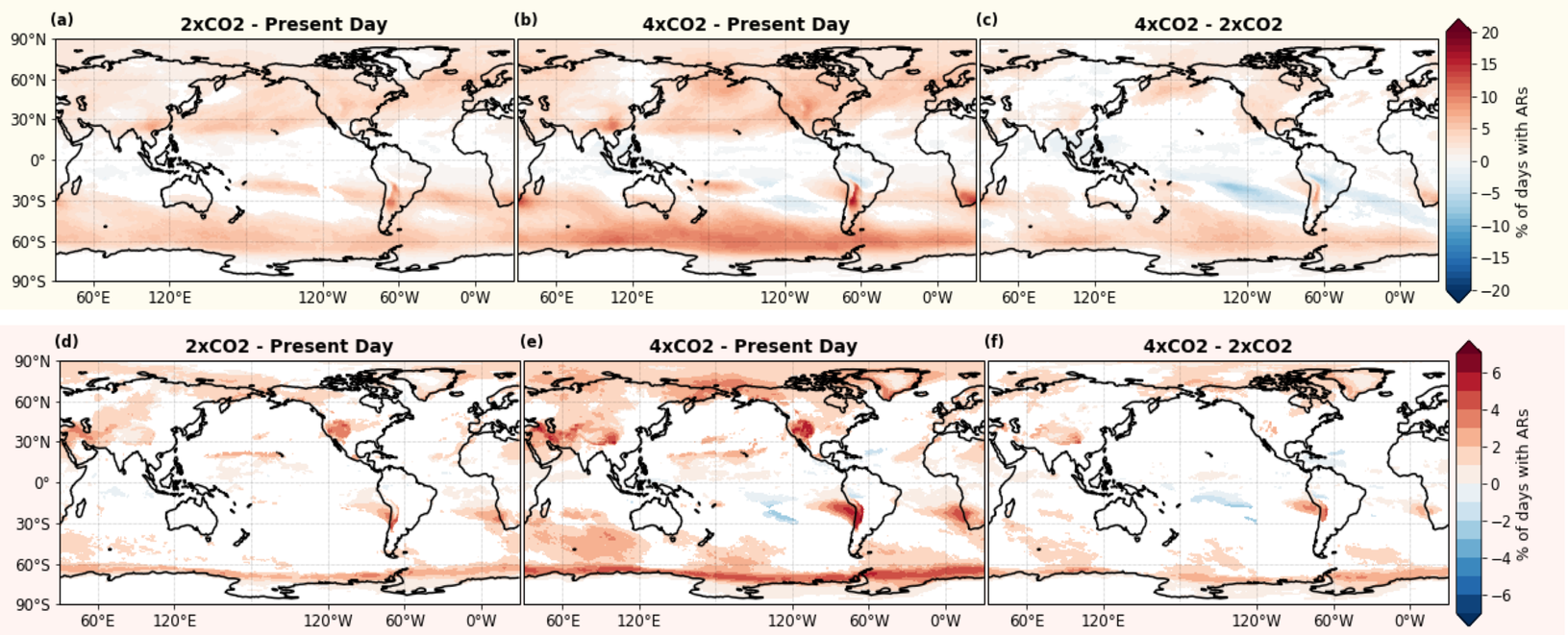

Figure 5: Changes in mean % of days with ARs using IVT threshold from present day simulation (a-c) and IVT threshold from corresponding simulation (d-f). Only values with 95% level statistical significance are shown.

Present Day Threshold: The IVT thresholds derived for present day simulation is used for the other two simulations. Significant increase can be seen almost everywhere around the globe.

Cons: Many regions with high IVT is not detected under enhanced GHG conditions as the it does not satisfy the present day constraints (the % of rejection increases for all the constraints)

Dynamic Threshold: For each scenario, IVT thresholds are derived separately. The magnitude of change is much smaller. Regions with high elevation stands out as the regions with strongest increases.

Cons: We are actually detecting structures with same statistical features compared to the mean state. Therefore, except for mean IVT transport, other characteristics remain very similar in both 2xCO2 and 4xCO2 conditions.

PS: See the attached video to see some snapshots of detected ARs using the two different thresholds

Response to GHG Forcing

Using PD Threshold

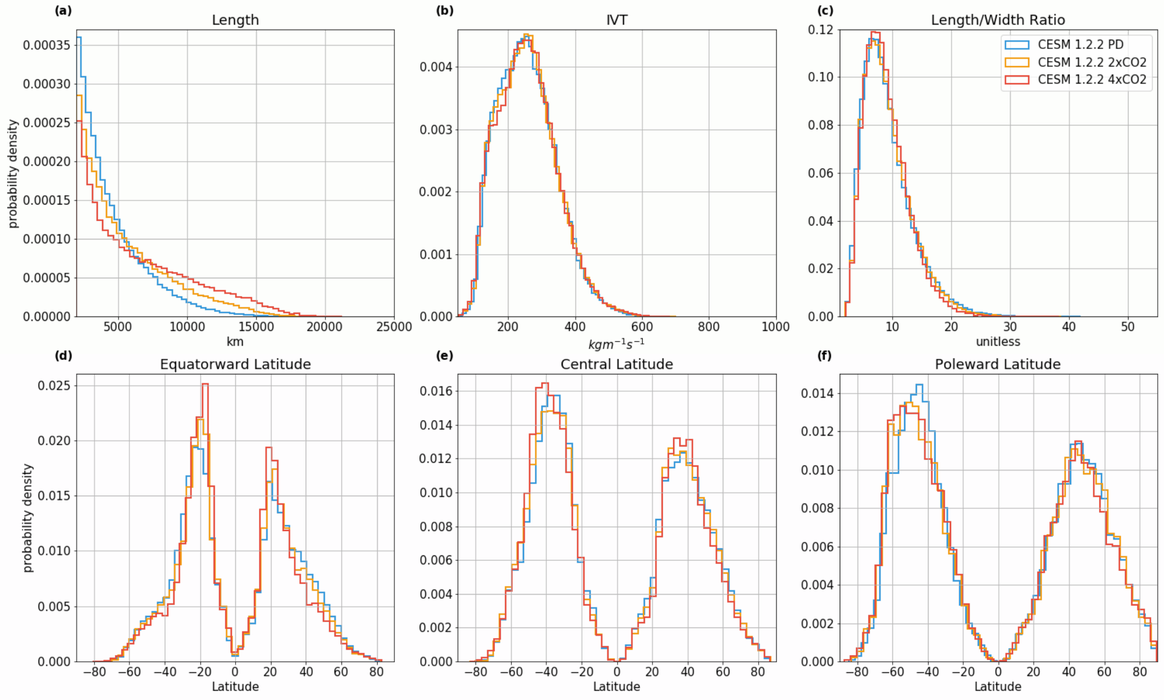

Figure 4: (a)-(f) shows the distribution of AR characteristics (Length, mean Integrated vapor transport, length/width ratio, position of centroid, equatorward latitude, poleward latitude) for PD (blue), 2CO2(orange) and 4CO2(red) using the thresholds from the PD runs.

Using Dynamic Threshold

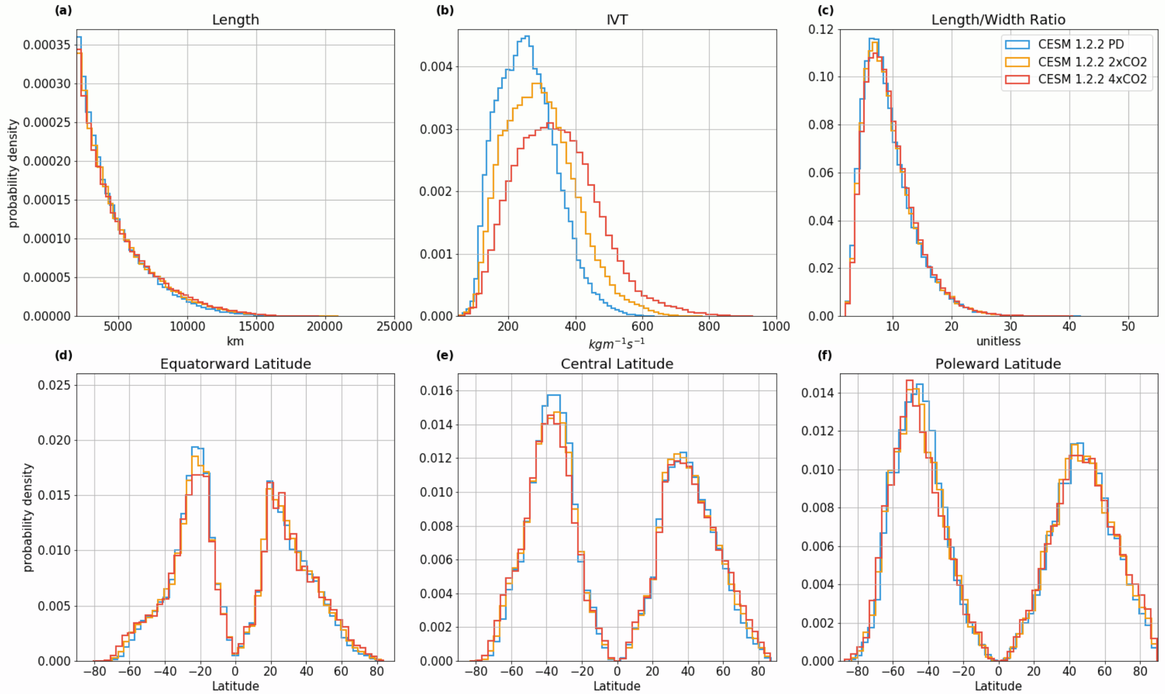

Figure 5: (a)-(f) shows the distribution of AR characteristics (Length, mean Integrated vapor transport, length/width ratio, position of centroid, equatorward latitude, poleward latitude) for PD (blue), 2CO2(orange) and 4CO2(red) using the thresholds from the corresponding runs.

SHAPE

LOCATION

Summary

Characteristics	2xCO2		4xCO2		Espinoza et.al. 2018
	Present Day Threshold	Future Threshold	Present Day Threshold	Future Threshold	(RCP 8.5)
Mean Global Frequency	Increase ~42%	Increase by ~11 %	Increase ~61%	Increase by ~19%	Increase by ~49%
Total Counts	Decrease by ~6%	Increase by ~3%	Decrease by ~30%	Increase by ~5%	Decrease by ~10 %
Mean Length	Increase by ~20%	Increase by ~4%	Increase by ~42%	Increase by ~5.7%	Increase by ~25%
Mean Width	Increase by ~18%	Increase by ~1.5%	Increase by ~42%	Increase by ~1.7%	Increase by ~25%
Total Landfalling counts	Increase by ~13.5%	Increase by ~9%	Increase by 4%	Increase by ~19%	-
Mean IVT Transport	Increase by ~2.5%	Increase by ~15%	Increase by ~4.4%	Increase by ~35%	Increase by 25%

Table 1: Changes seen in AR characteristics in response to GHG warming is summarized. A recently published study[6] is also included for reference

Conclusions and Caveats

1. In this preliminary study, we show the response of ARs to increased greenhouse gas forcing using AR detection methods developed by Guan and Waliser (2015).
2. The future changes in ARs are estimated using present-day thresholds as well as future thresholds. Although both methods show an enhanced AR activity, the magnitudes show a difference of the order of 10.
3. We would like to point out that, using present day thresholds or dynamic thresholds in a high resolution simulation may not lead to same conclusions. An impact based approach may help us to determine the suitable way of applying thresholds.
4. A lack of comprehensive theory governing the formation, maintenance and decay of ARs makes it harder to understand the response of AR. Some uncertainty is also introduced by the abundance of detection methods. Lagrangian Coherent Structures (LCS) analysis are being implemented to study these in detail.

References

1) Ralph, F. M., Dettinger, M. D., Cairns, M. M., Galarneau, T. J., & Eylander, J. (2018). Defining "atmospheric river": How the Glossary of Meteorology helped resolve a debate. Bulletin of the American Meteorological Society, 99(4), 837-839.
2) Zhu, Y., & Newell, R. E. (1998). A proposed algorithm for moisture fluxes from atmospheric rivers. Monthly weather review, 126(3), 725-735.
3) Ralph, F. M., & Dettinger, M. D. (2011). Storms, floods, and the science of atmospheric rivers. Eos, Transactions American Geophysical Union, 92(32), 265-266.
4) Small, R. J., Bacmeister, J., Bailey, D., Baker, A., Bishop, S., Bryan, F., ... & Jochum, M. (2014). A new synoptic scale resolving global climate simulation using the Community Earth System Model. Journal of Advances in Modeling Earth Systems, 6(4), 1065-1094.
5) Guan, B., & Waliser, D. E. (2015). Detection of atmospheric rivers: Evaluation and application of an algorithm for global studies. Journal of Geophysical Research: Atmospheres, 120(24), 12514-12535.
6) Espinoza, V., Waliser, D. E., Guan, B., Lavers, D. A., & Ralph, F. M. (2018). Global analysis of climate change projection effects on atmospheric rivers. Geophysical Research Letters, 45(9), 4299-4308.